HHS Public Access

Author manuscript

IEEE Trans Med Imaging. Author manuscript; available in PMC 2021 June 01.

Published in final edited form as:

IEEE Trans Med Imaging. 2020 June ; 39(6): 2025–2034. doi:10.1109/TMI.2019.2963083.

N-Phase Local Expansion Ratio for Characterizing Out-of-Phase Lung Ventilation

Wei Shao,
University of Iowa and is now with Stanford University, Stanford, CA 94305 USA

Taylor J. Patton,
University of Wisconsin and is now with University of Colorado, Anschutz Medical Campus, Aurora, CO 80045 USA

Sarah E. Gerard,
University of Iowa and is now with the Brigham and Women's Hospital, Boston, MA 02115 USA

Yue Pan,
Department of Electrical and Computer Engineering, University of Iowa, Iowa City, IA 52242 USA

Joseph M. Reinhardt [Fellow, IEEE],
Roy J. Carver Department of Biomedical Engineering, University of Iowa, Iowa City, IA 52242, USA

Oguz C. Durumeric,
Department of Mathematics, University of Iowa, Iowa City, IA 52242 USA

John E. Bayouth,
Department of Human Oncology, University of Wisconsin - Madison, Madison, WI 53792-0600 USA

Gary E. Christensen [Fellow, IEEE]
Department of Electrical and Computer Engineering, University of Iowa, Iowa City, IA 52242 USA

Abstract

Out-of-phase ventilation occurs when local regions of the lung reach their maximum or minimum volumes at breathing phases other than the global end inhalation or exhalation phases. This paper presents the N-phase local expansion ratio (LER_N) as a surrogate for lung ventilation. A common approach to estimate lung ventilation is to use image registration to align the end exhalation and inhalation 3DCT images and then analyze the resulting correspondence map. This 2-phase local expansion ratio (LER_2) is limited because it ignores out-of-phase ventilation and thus may underestimate local lung ventilation. To overcome this limitation, LER_N measures the maximum ratio of local expansion and contraction over the entire breathing cycle. Comparing LER_2 to LER_N provides a means for detecting and characterizing locations of the lung that experience out-of-phase ventilation. We present a novel in-phase/out-of-phase ventilation (IOV) function plot to

weishao@stanford.edu.

visualize and measure the amount of high-function IOV that occurs during a breathing cycle. Treatment planning 4DCT scans collected during coached breathing from 32 human subjects with lung cancer were analyzed in this study. Results show that out-of-phase breathing occurred in all subjects and that the spatial distribution of out-of-phase ventilation varied from subject to subject. For the 32 subjects analyzed, 50% of the out-of-phase regions on average were mislabeled as low-function by LER_2 (high-function threshold of 1.1, IOV threshold of 1.05). 4DCT and Xenon-enhanced CT of four sheep showed that LER_8 is more accurate than LER_2 for measuring lung ventilation.

Keywords

CT; functional avoidance; image registration; lung; out-of-phase ventilation; radiation therapy

I. Introduction

During normal tidal breathing, it is often assumed that the total lung volume increases monotonically during inhalation, reaching a maximum volume at the end of inhalation. Similarly, during exhalation, it is often assumed that the total lung volume decreases monotonically and reaches a minimum volume at end of exhalation. However, some local regions of the lung may reach the maximum and minimum volumes at different respiratory phases than the total lung volume [1]. We refer to this phenomena as “out-of-phase” ventilation.

It has long been established [2], [3] that the lung experiences nonuniform ventilation during normal breathing. There are a number of reasons why out-of-phase ventilation occurs which include natural asymmetries in the lung anatomy [4], regional variations in the lung tissue material properties [5], and pulmonary pathologies [6]. Previous work using image registration and cine CT data [1] has shown that the lung does not expand uniformly during breathing. The results in [1] show that the lung expands at different rates at different locations in the lung and the spatial pattern of expansion and contraction is repeatable from one breath to the next. The lung may be modeled as elastic material [7], [8] and has heterogeneous regional ventilation [3], [9], [10]. This indicates that air comes into different regions of the lung at different times and speeds during inhalation. Likewise, air leaves different regions of the lung at different times and speeds during exhalation. When the amount of ventilation heterogeneity is large enough, different regions of the lung may reach maximum and minimum volume at different times resulting in out-of-phase ventilation. Individuals have different amounts and magnitudes of ventilation heterogeneity, which leads to different amounts and magnitudes of out-of-phase ventilation.

Figure 1 illustrates a typical example of in-phase and out-of-phase ventilation that occurs during normal tidal breathing in a human subject measured using 4DCT and image registration. This figure shows the local volume change of two voxels in different lungs over a breathing cycle. Voxel-1 was located in the upper lobe of the left lung and voxel-2 was located in the upper lobe of the right lung. For uniform in-phase breathing, this graph would be a straight line from the volume at 0EX to the volume at 100IN and another straight line from 100IN back to 0EX. The graph of the volume for voxel-1 shows that it expanded and contracted in-phase with the global expansion and contraction of the lung, i.e., its maximum volume was reached at 100IN and its minimum volume was reached at 0EX. The volume of voxel-2 expanded out-of-phase with the expansion and contraction of the global lung, i.e., voxel-2 reached its maximum volume in phase 80IN and its minimum volume in phase 20EX.

We are interested in studying the spatial nature of out-of-phase breathing to assess local ventilation for a small number of subjects. For the rest of the paper, the terms lung function and lung ventilation will be used interchangeably. We acknowledge that there are other aspects of lung function, but we are ignoring them in this paper. Lung ventilation can be measured using ventilation scintigraphy, single photon emission computed tomography (SPECT), and positron emission tomography (PET). These techniques are often limited by low spatial resolution, high cost, long scan time, and/or low accessibility to patients [11].

An alternative approach that does not suffer from low spatial resolution is to estimate local lung ventilation from end inspiration and end expiration 3DCT image volumes. Reinhardt et al. and Ding et al. [12], [13] proposed an approach that used image registration to find a dense correspondence map between the end inspiration and end expiration phases. In this approach, the Jacobian determinant of the correspondence map is used to compute the local lung ventilation (i.e., the local expansion and contraction of the lung). We will refer to this approach as the 2-phase local expansion ratio (LER_2) since it is computed by registering two 3D CT image volumes. One limitation of this approach is that it assumes that all local regions of the lung reach their maximum and minimum volumes in the global end inhalation and exhalation breathing phases, respectively. In other words, it does not take into account out-of-phase breathing.

In this paper, we propose a new approach to measure local lung ventilation called the N-phase local expansion ratio (LER_N) that uses all N phases of a 4DCT scan of the lung to account for out-of-phase breathing. The LER_N approach calculates the maximum ratio of expansion to contraction over the breathing cycle at each point in the lung. The example in Fig. 1 illustrates the difference between computing lung function using LER_2 and LER_{10}. Using the LER_2 approach, voxel-1 and voxel-2 are assumed to have the same ventilation (function) since both expanded from a unit volume at the 0EX phase to a volume of 1.27 at the 100IN phase. On the other hand, LER_{10} uses 10 phases of the breathing cycle to assess lung function. Using LER_{10}, the full expansion of voxel-1 was 1.29/0.97 = 1.33 and the full expansion of voxel-2 was 1.27/1 = 1.27. Using LER_{10}, we may conclude that voxel-1 has higher function (increased ventilation) compared to voxel-2. Furthermore, this example shows that LER_2 underestimated the lung function of voxel-1.

To investigate the potential benefits of using LER_{10} compared to LER_2 for CT ventilation imaging, we analyzed 4DCT lung images collected from 32 human subjects undergoing RT for lung cancer. The results are presented in Section III. In this paper, we use LER_2 or LER_N as a surrogate of lung ventilation.

An earlier version of this paper was presented at the First International Workshop in Thoracic Image Analysis, Spain, 2018 [14].

II. Methods

A. Image Acquisition

1) Acquisition of 4DCT of Human Subjects: This study used 4DCT images from 32 human subjects (15 female and 17 male) who were undergoing RT and was approved by the University of Wisconsin institutional review board (protocol NCT02843568). All subjects in this study were diagnosed with lung cancer (30 non-small cell, 1 small cell, 1 endometrial cancer metastatic to the lung). The subject age (mean 70.1 +/− 9.0 years, range 52-89 years) and Karnofsky Performance Status (mean 90.6 +/− 9, range 70 100) were indicative of reasonable health. Subjects were predominately experiencing early stage non-small cell lung cancer: Stage I - 18, Stage II - 2, Stage III - 10, Stage IV 0; the small cell lung cancer subject had limited stage disease, and the endometrial cancer subject had Stage IIIB disease. Exclusion criteria included prior (within last 6 months) or future planned therapeutic surgery for the treatment of the existing lung cancer, prior thoracic radiotherapy, severe COPD defined as disease requiring an inpatient stay for respiratory deterioration within the past 3 months, oxygen dependence of more than 2 L/min continuously throughout the day at baseline, known underlying collagen vascular disease or intrinsic lung disease that could complicate expected sequelae of radiation (idiopathic pulmonary fibrosis, Wegeners granulomatosis), uncontrolled intercurrent illness including, but not limited to ongoing or active infection, symptomatic congestive heart failure, unstable angina pectoris, cardiac arrhythmia, or psychiatric illness/social situations that would limit compliance with study requirements. Two 4DCT scans were acquired for each subject before RT, with a 5-minute break between the two scans. The 4DCT data sets were acquired on a Siemens EDGE CT scanner using 120 kVp, 100 mAs per rotation, tube rotation period slightly greater than 0.5 seconds, 0.09 pitch, 76.8 mm beam collimation, 128 detector rows, and reconstructed slice thicknesses of 0.6 mm. Musical cues and voice instruction guidance were played throughout the scan to improve the repeatability of the respiratory pattern [15]. In our helical 4DCT acquisition, a reflective marker block is placed on the patient's abdomen and its height is tracked in real time by a camera-based system. The marker's height is recorded over several breathing cycles as the table moves and is used as a measure of respiratory magnitude. The observed image data is then sorted by this respiratory signal and reconstructed into a 4DCT scan containing 10 breathing phases, where each 3DCT image consists of several stacks acquired at different times. Each 4DCT data set was reconstructed into 10 breathing phases, with 20% (20IN), 40% (40IN), 60% (60IN), 80% (80IN) and 100% (100IN) of the respiratory period's amplitude inspiration phases and 80% (80EX), 60% (60EX), 40% (40EX), 20% (20EX) and 0% (0EX) of the respiratory period's amplitude expiration phases. The 32 subjects in this study were selected from a protocol with a larger cohort. Ten subjects that had major artifacts in 4DCT scans were excluded.

2) Acquisition of 4DCT and Xe-CT of Animal Subjects: Appropriate animal ethics approval was obtained for these protocols from the University of Iowa Animal Care and Use Committee and the study adhered to NIH guidelines for animal experimentation.

Respiratory-gated 4DCT and Xe-CT of four adult sheep were used in this study. Volumetric CT scans were acquired at different airway pressures with the sheep held apneic. An imaging protocol with slice collimation of 0.6 mm, pitch of 0.1, rotation time of 0.5 s, slice thickness of 0.75 mm, slice spacing of 0.5 mm, tube current of 100 mAs and tube voltage of 120kVp was used. A Siemens B30f kernel was used to retrospectively reconstruct 4DCT data of 25% (25IN), 50% (50IN), 75% (75IN), and 100% (100IN) inspiration phases and 75% (75EX), 50% (50EX), 25% (25EX), and 0% (0EX) expiration phases. A portion of the lung of about 3 cm thick in the axial direction was selected for Xe-CT imaging near 0EX phase. Xe-CT scans were acquired by setting the scanner in ventilation triggering mode, typically with 80 KeV energy, 160 mAs tube current, a 360° rotation and a 0.33 s scan time. A slab of 12 contiguous axial Xe-CT slices was acquired for 45 breathing cycles as xenon gas washes into the lung. For each voxel inside the lung, we fitted an exponential growth model to the wash-in Xenon gas density change. The inverse of the time constant of the exponential growth was used as a measure of lung function at that voxel. More details of the imaging protocols can be found in our previous publication [12].

B. Image Registration

The sum of squared tissue volume difference (SSTVD) image registration algorithm [16] was used to register lung CT volumes. This algorithm was chosen since it models the CT intensity change of the lung associated with breathing. A detailed comparison of the accuracy of the sum of squared differences, mutual information and SSTVD similarity cost functions for lung image registration can be found in [17]. The SSTVD image registration algorithm has been shown to have sub-voxel accuracy [18], [19]. A brief overview of the algorithm follows.

Let $\Omega \subset \mathbb{R}^3$ represent the domain or coordinate system of a 3D CT image to be registered. SSTVD image registration estimates a smooth one-to-one correspondence map $\phi : \Omega \to \Omega$ between a fixed image $I_f : \Omega \to \mathbb{R}$ and a moving image $I_m : \Omega \to \mathbb{R}$ that minimizes the cost function

$$C(I_f, I_m) = C_{SSTVD}(I_f, I_m) + \lambda \cdot Reg(\phi) \tag{1}$$

where C_{SSTVD} is the SSTVD similarity cost, $Reg(\phi)$ is the regularization cost and λ is the regularization weight. The CT image in Housfield unit (HU) is converted into a tissue fraction/density image by:

$$\text{Tissue Fraction} = \frac{HU - HU_{air}}{HU_{tissue} - HU_{air}} = \frac{HU + 1000}{1055} \tag{2}$$

where the HUs of tissue and air are approximately $HU_{tissue} = 55$ and $HU_{air} = -1000$. The tissue fraction images associated with I_f and I_m are denoted by R_f and R_m, respectively, i.e., $R_f = \frac{I_f + 1000}{1055}$ and $R_m = \frac{I_m + 1000}{1055}$. The sum of squared tissue volume difference (SSTVD) similarity metric [16], [18], [20] is given by

$$C_{SSTVD} = \int_{\Omega} \left(R_f(x) - |J_\phi|(x) \times R_m(\phi(x))\right)^2 dx\,. \tag{3}$$

The regularization cost is given by

$$Reg(\phi) = \int_{\Omega} \left\| c_1(\nabla \cdot \nabla)u(x) + c_2 \nabla(\nabla \cdot u(x)) \right\|^2 dx. \tag{4}$$

where $\nabla = \left[\frac{\partial}{\partial x_1}, \frac{\partial}{\partial x_2}, \frac{\partial}{\partial x_3}\right]^T$, ∇ is the divergence operator and $u = \phi$ - Id is the associated displacement vector field, where Id is the identity map. The values $c_1 = 0.75$ and $c_2 = 0.25$ were used in this study.

The nonrigid transformation ϕ was parameterized by uniform cubic B-splines. A multi-resolution multi-grid framework was used in the C++ implementation of the registration method. Six resolution levels were used, the final B-spline grid spacing was 4x4x4 voxels, and the final image resolution was 2x2x2 voxels. A Broyden-Fletcher-Goldfarb-Shanno (LBFGS) optimizer was used for limited memory consumption and rapid convergence.

C. 2-Phase Local Expansion Ratio (LER_2)

The 2-phase local expansion ratio (LER_2) was computed following the approach of Reinhardt et al. [12] and Ding et al. [13]. In this approach, local ventilation is estimated by first estimating a transformation (i.e., dense correspondence map) between the end inspiration and end expiration lung CT image volumes and then taking the Jacobian determinant of the transformation. SSTVD image registration was used to estimate a nonrigid pullback transformation ϕ that transforms the 100IN phase to look like the 0EX phase. The domain of the pullback transformation ϕ is the coordinate system of the 0EX phase and its range is the coordinate system of the 100IN phase, i.e., $y = \phi(x)$ maps a point x defined in the 0EX coordinate system to its corresponding location y in the 100IN phase. LER_2 measures the expansion of the lung at each point x and is given by

$$LER_2(x) \triangleq \left|J_\phi(x)\right|/1 \tag{5}$$

where $|J_\phi|$ is the determinant of the Jacobian matrix. Equation (5) is the ratio of a transformed unit volume of tissue to its original unit volume. The Jacobian matrix J_ϕ of the transformation ϕ is given by:

$$J_\phi \triangleq \begin{bmatrix} \frac{\partial \phi_1}{\partial x_1} & \frac{\partial \phi_1}{\partial x_2} & \frac{\partial \phi_1}{\partial x_3} \\ \frac{\partial \phi_2}{\partial x_1} & \frac{\partial \phi_2}{\partial x_2} & \frac{\partial \phi_2}{\partial x_3} \\ \frac{\partial \phi_3}{\partial x_1} & \frac{\partial \phi_3}{\partial x_2} & \frac{\partial \phi_3}{\partial x_3} \end{bmatrix}. \tag{6}$$

The derivatives in the Jacobian matrix were computed numerically by the symmetric difference.

D. N-Phase Local Expansion Ratio (LER_N)

The proposed LER_N measure uses all N phases of a 4DCT scan to estimate the LER. Calculation of the LER_N involves estimating the local lung volume in each respiratory phase. This is achieved by performing pairwise registrations from each breathing phase to the 0EX phase as shown in Fig. 2. The Jacobian determinant of the pullback transformation ϕ_i from the i^{th} breathing phase to the 0EX phase is denoted by $J_i(x) = |\mathrm{J}_{\phi_i}(x)|$. For $i = 0$, $J_0(x) = |\mathrm{J}_{\phi_0}(x)| \triangleq 1$ is the Jacobian determinant of the identity map, i.e., the Jacobian determinant of the map from 0EX to 0EX. Note that the values of the Jacobian determinant image J_i represents the pointwise lung volume expansion in the i^{th} breathing phase with respect to the 0EX phase. LER_N is defined at $x \in \Omega$ by

$$LER_N(x) \triangleq \max_{i \in \{0, \cdots, N-1\}} J_i(x) / \min_{j \in \{0, \cdots, N-1\}} J_j(x) \quad (7)$$

where N denotes the number of breathing phases of a 4DCT scan. Note that this definition implies that $LER_N \geq LER_2$ where equality holds if and only if the lung was breathing in phase at the point x.

We note that LER_N is more computationally intensive than LER_2, because it requires deformable image registration for N-1 pairs of image datasets, whereas LER_2 only requires one registration.

E. In-phase/Out-of-phase Ventilation (IOV) Threshold

Comparing LER_N to LER_2 provides a means for detecting and characterizing locations of the lung that experience out-of-phase ventilation. One may naively define out-of-phase ventilation when LER_N is greater than LER_2. However, LER_N and LER_2 both suffer from measurement error due to variation in breathing and errors in image registration. The effect of measurement error is to over estimate the amount of the lung that is out-of-phase. To reduce the problem of overestimation, we define a region of the lung to be out-of-phase if

$$LER_N > T \times LER_2 \quad (8)$$

for the IOV threshold $T \geq 1$. The value of T specifies a confidence level that LER_N differs sufficiently from LER_2 to label a region as out of phase. We used an IOV threshold value of $T = 1.05$ for the results presented in this paper. See Section IV-B for a discussion of threshold sensitivity.

III. Results

For each 4DCT data set (see Section II-A), the respiratory phase was registered to the 0EX phase using SSTVD pairwise registration as discussed in Section II-B and illustrated in Fig. 2. LER_2 and LER_{10} were computed using (5) and (7), respectively.

A. Image Registration Accuracy

The accuracy of LER_{10} and LER_2 calculations depends on the accuracy of the image registration. The SSTVD image registration algorithm used in this paper has been shown to have sub-voxel accuracy [18], [19]. For quality control purpose, we investigated image registration accuracy for 5 out of the 32 subjects. We used a landmark construction tool developed by Murphy et al. [21] to automatically choose a well-distributed set of 100 landmarks in the end-exhale CT. The corresponding landmarks in the end-inhale CT were manually labeled by an expert. The mean landmark errors (MLEs) for those 5 subjects were 1.10, 0.76, 1.56, 1.35, and 1.26 in voxels, with mean MLE equal to 1.21 voxels (which were 1mm sided cubes).

B. Spatial Distribution of Out-of-Phase Breathing

The spatial distribution of out-of-phase ventilation can be visualized by displaying the ratio of LER_{10} to LER_2. The larger this ratio is, the larger the out-of-phase ventilation is. Figure 3 shows the spatial distribution and magnitude of out-of-phase ventilation for 14 of the 32 subjects. The color bar is graduated from green to yellow to red corresponding to different IOV threshold values from 1.0 to 1.1. Regions colored green show in-phase ventilation, i.e., they shown agreement between LER_{10} and LER_2 and indicate regions of the lung that had peak expansion from 0EX to 100IN. Regions colored yellow to orange are regions transitioning from in-phase breathing to out-of-phase breathing. Regions colored red are regions of the lung that are clearly ventilating out-of-phase. These images show that all subjects had some degree of out-of-phase ventilation. They also show that out-of-phase ventilation is subject specific and are distributed throughout the lung.

Although out-of-phase ventilation seems to more likely to occur in the basal part of the lung, a detailed analysis of the spatial distribution of out-of-phase ventilation requires further study. All the subjects studied in this work had lung cancer. Further study is required to understand the relationship between the location of the tumor and the spatial distribution of out-of-phase ventilation. Likewise, further study is required to study how the spatial distribution of pulmonary comorbidities such as emphysema, COPD, and fibrosis may affect out-ofphase lung ventilation. For example, fibrotic lung regions experience less expansion and contraction over the breathing cycle compared to healthy lung tissue and thus will affect the spatial pattern of out-of-phase breathing accordingly. In addition, further study is required to investigate what effect the motion of the heart has on out-of-phase ventilation in regions of the lung near the heart.

C. In-Phase/Out-of-Phase Ventilation (IOV) Function Plot

Figure 4 shows the in-phase/out-of-phase ventilation (IOV) function plots for 4 of the 32 subjects. An IOV plot is a 2D histogram of LER_{10} versus LER_2. A logarithmic scale was used for visualization. The functions $y = x$ and $y = 1.05x$ are overlaid on the histogram to partition the plot into in-phase and out-of-phase regions. The function $y = x$ corresponds to $LER_{10} = LER_2$. By definition, all points lie above the $y = x$ solid line since $LER_{10} \geq LER_2$. Points that lie above the $y = 1.05x$ solid line (i.e., points above the IOV threshold of 1.05) are defined to be out-of-phase and points that lie between the two lines are defined to be in-phase.

The 2D plane in Fig. 4 is divided into four regions: A, B, C and D. Region A corresponds to in-phase ventilation and regions B, C and D correspond to out-of-phase ventilation. High-function regions are defined as regions that have volume change greater than 1.1 whereas low-function regions have volume change less than 1.1. The 1.1 threshold used to define regions of high ventilation/function was chosen to match our prior work [22]. When comparing lung tissue mechanics changes following radiation therapy, lung regions with Jacobian value > 1.1 displayed significantly greater reduction in elasticity for the same radiation dose, when compared to regions with a Jacobian < 1.1. LER_2 defines points to the right of the 1.1 vertical line as high function whereas points to the left are defined as low function. Likewise, LER_{10} defines points above the 1.1 horizontal line as high function whereas points below this line are defined as low function. Lung function is characterized as low-function by both LER_2 and LER_{10} in region B. Lung function is characterized as low-function by LER_2 whereas high-function by LER_{10} in region C. Finally, lung function is characterized as high-function by both LER_2 and LER_{10} in region D. In summary, region B and region D are characterized the same by LER_2 and LER_{10} as low-function and high-function, respectively. On the other hand, region C is characterized as high-function by LER_{10} and mischaracterized as low function by LER_2.

Figure 5 shows the in-phase/out-of-phase ventilation (IOV) functional plot for all 32 subjects. The IOV functional plot shown in Figure 5 is the cumulative 2D histogram of LER_2 versus LER_{10} computed from all 32 subjects. $P(A)$, $P(B)$, $P(C)$, and $P(D)$ denote the percentages of the voxels in regions A, B, C and D, respectively. On average for the 32 subjects, 78.7% of all voxels were in region A, i.e., 78.7% of the lung had in-phase ventilation using an out-of-phase threshold of 1.05. Conversely, on average 21.3% of the lung had out-of-phase ventilation. There were 3.4% of all voxels in region B, i.e., on average 16% of the out-of-phase ventilation was labeled as low-function by both LER_2 and LER_{10}. There were 10.6% of all voxels in region C, i.e., on average 50% of the out-of-phase ventilation was mislabeled as low-function by LER_2 but was correctly labeled as high-function by the LER_{10}. There were 7.3% of all voxels were in region D, i.e., on average 34% of the out-of-phase ventilation was labeled as high-function by both LER_2 and LER_{10}.

Table I summarizes the percentages of the lung volume for regions A, B, C and D for each of the 32 subjects. This table shows that all subjects had some degree of out-of-phase ventilation. The average percentages for regions A, B, C, and D reported in Table I are slightly different from 78.7% in Fig. 5. This is because percentages in Fig. 5 were calculated using all lung voxels in the population whereas the computations used to generate Table I were normalized to 100% for each subject.

D. LER_N Validation

Specific ventilation derived from Xenon-enhanced CT (Xe-CT) is considered to be a gold standard for ventilation imaging modalities [23]. We used 4DCT and Xe-CT of four sheep to evaluate the accuracy of LER_2 and LER_8 to estimate lung ventilation. For each sheep, the Spearman correlation coefficient of Xe-CT specific ventilation with LER_2 and with LER_8 in out-of-phase regions are shown in Table II. The mean Spearman correlation coefficients for LER_2 and LER_8 in out-of-phase regions are 0.436 and 0.486, respectively. Since the correlation between LER_8 and Xe-CT specific ventilation is 11.5% higher than the correlation between LER_2 and Xe-CT specific ventilation, we conclude that the LER_8

measure is more accurate than the LER_2 measure when quantifying lung function of the four sheep. Previous work reported that the mean Spearman's correlation between LER_2 and Xe-CT specific ventilation was 0.44 [24].

One way to put the LER_8 correlation coefficient of 0.486 in perspective is to note that the LER_2 method was judged to be the most accurate method for estimating ventilation from CT images in the 2019 AAPM Computed Tomography Ventilation Imaging Evaluation 2019 (CTVIE19) Grand Challenge (publication pending). This competition was the largest competition of its kind to date consisting of 44 teams (23 of which finished the competition) from around the world and required registration of 445 inspiration and expiration CT scans collected from over 20 different research centers. We could not evaluate the LER_N approach on this challenge data set since it only consisted of pairs of CT images. To clarify, some of the challenge data sets were actually 4DCT images, however, only two phases, the end expiration and end inspiration, were released to the public as the challenge data.

IV. Discussion

A. Potential Clinical Impact

This work has the potential to improve functional avoidance radiotherapy. Radiation therapy is used to treat nearly 75% of all lung cancers [25]. Functional avoidance RT reduces the risk of radiation-induced lung injury by avoiding irradiating high-function lung tissues (i.e., regions of high ventilation) [26]–[34]. Previous work shows that high-function lung tissues are more susceptible to radiation damage than low-function lung tissues [22]. A study conducted by Yamamoto et al. [11] showed that functional avoidance RT planning significantly reduced doses to high-function lung regions without increasing doses to other critical organs.

Figure. 6 shows transverse CT images of the lung of a patient with lung cancer. Overlaid contours show the radiation dose plans for conventional, LER_2-derived functional avoidance, and LER_N-derived functional avoidance. The smallest isodose curve (yellow) encompasses the tumor. The colored regions show the functional avoidance maps where red corresponds to high functioning regions and purple and blue corresponds to low functioning regions. This figure shows that the LER_N-derived plan is better than both the LER_2 and conventional methods. The LER_N has better coverage of the tumor than the LER_2 plan whereas at the same time having comparable coverage of the tumor to the conventional plan. Also notice that the LER_N plan delivered less radiation dose to the normal left lung than the conventional and LER_2 plans. Finally, the dose volume histograms (not shown in this paper) show that the LER_N method delivered more dose to the tumor and less dose to the anatomy to be avoided than both the conventional and LER_2 dose plans for the subject illustrated in Fig. 6.

B. In-Phase/Out-of-phase Ventilation (IOV) Threshold

The in-phase/out-of-phase (IOV) threshold value T in (8) is used to partition the lung into in-phase and out-of-phase regions. In this section, we investigate the sensitivity of T to the percentage of lung that is defined as out-of-phase. To study the sensitivity of T, we constructed the complementary cumulative distribution function (CCDF) for the 32 human subjects in this study (see Fig. 7). In this context, a CCDF is a plot of the percentage of out-of-phase lung volume versus the threshold value T. We refer to such a CCDF as a IOV threshold sensitivity plot. The thick black line in Fig. 7 corresponds to the average of the 32 plots.

By definition, $LER_{10} > T \times LER_2$ for values of $T < 1$, i.e., 100% of the lung is defined to be out-of-phase for $T < 1$. At $T = 1$, all the IOV threshold sensitivity plots have a discontinuity due to out-of-phase ventilation (See Fig. 7). On average, approximately 55% of the lung is considered as out-of-phase for $T = 1$. A value of $T = 1$ is not a useful threshold to define out-of-phase ventilation for the data sets studied because it would mean that more of the lung is out-of-phase than in-phase. This would contradict the definitions of the end inhale and exhale phases. Thus, a value of $T > 1$ should be chosen as the IOV threshold.

Choosing a biologically relevant value of the IOV threshold T is beyond the scope of this paper since the number of data sets we studied is too small to make any conclusions and all the data sets studied were from a population of individuals with lung cancer. In our future work, we plan to investigate this question on a larger data set that includes healthy subjects and to validate our choice of threshold with an independent measure of out-of-phase ventilation. In this work, we choose the threshold value to be 1.05 based on the average curve in Fig. 7 to reflect Jacobian determinant values that were not due to measurement error. Based on this threshold, we concluded that on average 20.2% of the lung for the individuals studied had out-of-phase ventilation. The IOV threshold determines the percentage of lung with out-of-phase ventilation. For example, if we choose $T = 1.1$, then on average 8.8% of the lung would be designated as out-of-phase.

C. Dependence of LER_N on Image Registration Algorithm

Jacobian measurements have been shown to be sensitive to image registration algorithms [35]–[37]. To test the sensitivity of our results to registration algorithms, we used the Elastix image registration software [38] to rerun all pairwise registrations. Instead of SSTVD, the mutual information was used as the similarity metric. We used a different multiresolution scheme and a different optimizer (standard gradient descent). Using the Elastix toolbox, we found that at a 1.05 out-ofphase threshold, 24.2% (compared to 20.2% using SSTVD) of the lung had out-of-phase ventilation. The mean Dice coefficient of the out-of-phase images computed from two different registration algorithms was 0.65. Fig. 8 shows the IOV spatial images of a typical subject computed using both image registration algorithms. Fig. 9 shows the IOV function plots for both registration algorithms. These results show that both image registration algorithms produce similar out-of phase images.

D. Choice of LER_N Coordinate System

The definition of LER_N is independent of the choice of the reference coordinate system in which it is calculated (See Fig. 2). This can be seen with the following example. Consider a 4DCT scan of three breathing phases and suppose the volume of a voxel at those phases are 1, 2, 4, respectively. If the first breathing phase was chosen as the reference, the three Jacobian values used in (7) are 1, 2, 4, and $LER_3 = \frac{max\{1,2,4\}}{\min\{1,2,4\}} = \frac{4}{1} = 4$. If the second breathing phase was chosen as the reference, the three Jacobian values are 0.5, 1, 2 and $LER_3 = \frac{max\{0.5, 1, 2\}}{\min\{0.5, 1, 2\}} = \frac{2}{0.5} = 4$ similarly if the third breathing phase was chosen as the reference, we have $LER_3 = \frac{max\{0.25, 0.5, 1\}}{\min\{0.25, 0.5, 1\}} = \frac{1}{0.25} = 4$. This example show that the computation of LER_3 at this voxel is independent of the reference coordinate system.

We now present a formal proof. Assume that ϕ_i for $i = 0, \ldots, N-1$ are given with respect to coordinate system 0 as in Fig. 2 and that we want to calculate the LER_N in the coordinate system of breathing phase j. The transformations from phase i to phase j are given by $\psi_{ij} = \phi_i \circ \phi_j^{-1}$. The Jacobian determinate of transformation ψ_{ij} at the point y is given by $J(\psi_{ij}(y)) = J(\phi_i \circ \phi_j^{-1}(y))$. LER_N given in the coordinate system of phase j is

$$
\begin{aligned}
LER_N(y) &= \frac{max_{m \in \{0, \cdots, N-1\}} J(\psi_{mj}(y))}{\min_{n \in \{0, \cdots, N-1\}} J(\psi_{nj}(y))} \\
&= \frac{max_{m \in \{0, \cdots, N-1\}} J(\phi_m \circ \phi_j^{-1}(y))}{\min_{n \in \{0, \cdots, N-1\}} J(\phi_n \circ \phi_j^{-1}(y))}
\end{aligned}
$$

Substituting $y = \phi_j(x)$ into the previous equation gives (7). In other words, $\text{LER}_N(y)$ computed in phase j is just a transformed version of $\text{LER}_N(x)$ computed in phase 0 by the transformation $y = \phi_j(x)$.

The statement that the definition of LER_N is coordinate system independent does not mean that there is not coordinate system bias in practice. LER_N coordinate system bias will result from the registration algorithm used, registration errors, and lack of inverse consistency and transitivity of the transformations. Bias in the LER_N calculation will also result from motion artifacts, partial volume effects, and noise in the reference phase image. Image registration from full inspiration to full expiration is preferable when registering lung images since it is easier to compress features such as airways in a digital image than to expand airways. For example small airways that are visible in the full inspiration phase are not visible in the full expiration phase. One way to think of this is that there are more samples (more voxels) of the lung when it is expanded compared to when it is compressed. In Fig. 2 all the phase images were registered to the 0EX phase so that the larger lung images were registered to the smaller lung image.

E. Lower Bounds of LER_N

LER_N for $N > 2$ has two lower bounds. The first lower bound is LER_2, because $LER_N \geq LER_2$ by definition. The second lower bound is $\frac{1}{LER_2}$ and it occurs when the maximum Jacobian determinant of the phase transformations is equal to 1. In this case, $\frac{1}{LER_2}$ represents the ratio of local lung volume in the 0EX phase to local lung volume in the 100IN phase. Thus, $\text{LER}_N \geq \frac{1}{LER_2}$. Therefore, $LER_N \geq \max\{LER_2, 1/LER_2\}$, i.e., LER_2 and $\frac{1}{LER_2}$ are lower bounds of LER_N. We define $x \triangleq LER_2$ and $y \triangleq LER_N$. The contour lines $y = x$ and $y = \frac{1}{x}$ in the cumulative 2D histogram of LER_2 versus LER_{10} in Fig. 5 correspond to the lower bounds LER_2 and $\frac{1}{LER_2}$, respectively. Notice that when $x < 1$, the contour line $y = \frac{1}{x}$ looks like the −45-degree line $y = -x+2$. The reason for this is as follows. By Taylor expansion of the function of $y = \frac{1}{x}$ at $x = 1$, we have $\frac{1}{x} \approx 1 + (-1)(x - 1) = -x + 2$ when x is close to 1.

V. Conclusions

This paper presented the N-phase local expansion ratio (LER_N) for characterizing lung ventilation. The LER_N approach was validated using Xenon-enhanced CT (Xe-CT) data collected from sheep on a ventilator. This data is considered a gold standard for ventilation imaging modalities [23]. LER_N was shown to have a higher correlation with Xe-CT than the traditional 2-phase local expansion ratio (LER_2).

In-phase/out-of-phase ventilation (IOV) images showed that all 32 human subjects studied experienced out-of-phase ventilation and that the location of the out-of-phase ventilation was subject specific. In-phase/out-of-phase ventilation (IOV) function plots where used to characterize the percentage of in-phase and out-of-phase ventilation and the percent of low versus high functioning regions of the lung. The IOV function plots demonstrated that a substantial volume of the lung was mischaracterized as low function by LER_2 but was considered high function by LER_N. For the 32 subjects analyzed, 50% of the out-of-phase regions on average were mislabeled as low-function by LER_2 (high-function threshold of 1.1, IOV threshold of 1.05).

We demonstrated that LER_N computed using different image registration algorithms predicted similar out-of-phase ventilation. Finally, we showed that in theory that LER_N is independent of the coordinate system used as the reference.

Acknowledgments

This work was supported in part by National Cancer Institute under award numbers R01CA166703 and R01CA166119.

References

[1]. Christensen GE, Song JH, Lu W, Naqa IE, and Low DA, "Tracking lung tissue motion and expansion/compression with inverse consistent image registration and spirometry." Medical Physics, vol. 34, no. 6, pp. 2155–2165, 6 2007. [PubMed: 17654918]

[2]. Rauwerda PE, "Unequal ventilation of different parts of the lung and the determination of cardiac output," Groningen: Thesis, State University Groningen, 1946.

[3]. Bates JHT, Lung Mechanics: An Inverse Modeling Approach. Cambridge University Press, 2009.

[4]. Leary D, Winkler T, Braune A, and Maksym GN, "Effects of airway tree asymmetry on the emergence and spatial persistence of ventilation defects," Journal of applied physiology, vol. 117, no. 4, pp. 353–362, 2014. [PubMed: 24947031]

[5]. MEAD J, "Mechanical properties of lungs," Physiological reviews, vol. 41, no. 2, pp. 281–330, 1961. [PubMed: 13768766]

[6]. Verbanck S, Paiva M, Schuermans D, Malfroot A, Vincken W, and Vanderhelst E, "Acinar and conductive ventilation heterogeneity in severe cf lung disease: Back to the model," Respiratory Physiology & Neurobiology, vol. 188, no. 2, 2013.

[7]. Naini AS, Patel RV, and Samani A, “Measurement of lung hyperelastic properties using inverse finite element approach,” IEEE Transactions on Biomedical Engineering, vol. 58, no. 10, pp. 2852–2859, 2011. [PubMed: 21724500]

[8]. Zeng YJ, Yager D, and Fung YC, “Measurement of the mechanical properties of the human lung tissue,” Journal of biomechanical engineering, vol. 109, no. 2, 1987.

[9]. Vogt B, Pulletz S, Elke G, Zhao Z, Zabel P, Weiler N et al., “Spatial and temporal heterogeneity of regional lung ventilation determined by electrical impedance tomography during pulmonary function testing,” Journal of applied physiology, vol. 113, no. 7, pp. 1154–1161, 2012. [PubMed: 22898553]

[10]. Robertson HT, Kreck TC, and Krueger MA, “The spatial and temporal heterogeneity of regional ventilation: Comparison of measurements by two high-resolution methods,” Respiratory Physiology & Neurobiology, vol. 148, no. 1, pp. 85–95, 2005. [PubMed: 15964251]

[11]. Yamamoto T, Kabus S, Von Berg J, Lorenz C, and Keall PJ, “Impact of four-dimensional computed tomography pulmonary ventilation imaging-based functional avoidance for lung cancer radiotherapy,” International Journal of Radiation Oncology* Biology* Physics, vol. 79, no. 1, pp. 279–288, 2011.

[12]. Reinhardt JM, Ding K, Cao K, Christensen GE, Hoffman EA, and Bodas SV, “Registration-based estimates of local lung tissue expansion compared to xenon-CT measures of specific ventilation,” Medical Image Analysis, vol. 12, no. 6, pp. 752–763, 2008. [PubMed: 18501665]

[13]. Ding K, Cao K, Fuld MK, Du K, Christensen GE, Hoffman EA et al., “Comparison of image registration based measures of regional lung ventilation from dynamic spiral ct with xe-ct,” Medical physics, vol. 39, no. 8, pp. 5084–5098, 2012. [PubMed: 22894434]

[14]. Shao W, Patton TJ, Gerard SE, Pan Y, Reinhardt JM, Bayouth JE et al., “Detecting out-of-phase ventilation using 4DCT to improve radiation therapy for lung cancer,” in Image Analysis for Moving Organ, Breast, and Thoracic Images, 2018, pp. 251–259.

[15]. Bayouth J, Patton T, Gerard S, Shao W, Christensen G, Reinhardt J, et al., “Signal processing analysis of breathing rates show improved spectral coherence when human subjects receive musical melody and voice instruction guidance.” Medical Physics, vol. 45, pp. E491–E491, 2018.

[16]. Yin Y, Hoffman EA, and Lin C-L, “Mass preserving non-rigid registration of CT lung images using cubic B-spline,” Medical Physics, vol. 36, no. 9, pp. 4213–4222, 2009. [PubMed: 19810495]

[17]. Cao K, “Mechanical analysis of lung ct images using nonrigid registration,” Ph.D. dissertation, The University of Iowa, Iowa City, IA 52242, 5 2012.

[18]. Cao K, Ding K, Christense GE, and Reinhardt JM, “Tissue volume and vesselness measure preserving nonrigid registration of lung CT images,” in Proc. SPIE, vol. 7623, 2010, p. 762309.

[19]. Cao K, Du K, Ding K, Reinhardt J, and Christensen G, “Regularized nonrigid registration of lung ct images by preserving tissue volume and vesselness measure,” in Med. Image Anal. Clinic: A Grand Challenge, 01 2010, pp. 43–54.

[20]. Gorbunova V, Lo P, Ashraf H, Dirksen A, Nielsen M, and de Bruijne M, “Weight preserving image registration for monitoring disease progression in lung CT,” in MICCAI, vol. 5242, 2008, pp. 863–870.

[21]. Murphy K, van Ginneken B, Pluim JPW, Klein S, and Staring M, “Semi-automatic reference standard construction for quantitative evaluatoin of lung CT registration,” in MICCAI, vol. 5242, 2008, pp. 1006–1013.

[22]. Patton TJ, Gerard SE, Shao W, Christensen GE, Reinhardt JM, and Bayouth JE, “Quantifying ventilation change due to radiation therapy using 4DCT Jacobian calculations,” Medical Physics, vol. 45, no. 10, pp. 4483–4492, 2018. [PubMed: 30047588]

[23]. Chon D, Simon BA, Beck KC, Shikata H, Saba OI, Won C et al., “Differences in regional wash-in and wash-out time constants for xenon-ct ventilation studies,” Respiratory physiology & neurobiology, vol. 148, no. 1, pp. 65–83, 2005. [PubMed: 16061426]

[24]. Zhang GG, Latifi K, Du K, Reinhardt JM, Christensen GE, Ding K et al., “Evaluation of the Δv 4d ct ventilation calculation method using in vivo xenon ct ventilation data and comparison to other methods,” Journal of Applied Clinical Medical Physics, vol. 17, no. 2, pp. 550–560, 2016.

[25]. Delaney G, Barton M, Jacob S, and Jalaludin B, “A model for decision making for the use of radiotherapy in lung cancer,” Lancet Oncology, vol. 4, no. 2, pp. 120–128, 2003. [PubMed: 12573354]

[26]. Christian JA, Partridge M, Nioutsikou E, Cook G, Mcnair HA, Cronin B et al., “The incorporation of spect functional lung imaging into inverse radiotherapy planning for non-small cell lung cancer,” Radiotherapy and Oncology, vol. 77, no. 3, pp. 271–277, 2005. [PubMed: 16274762]

[27]. Lavrenkov K, Christian JA, Partridge M, Niotsikou E, Cook G, Parker M et al., “A potential to reduce pulmonary toxicity: The use of perfusion spect with imrt for functional lung avoidance in radiotherapy of non-small cell lung cancer,” Radiotherapy and Oncology, vol. 83, no. 2, pp. 156–162, 2007. [PubMed: 17493699]

[28]. Siva S, Thomas R, Callahan J, Hardcastle N, Pham D, Kron T et al., “High-resolution pulmonary ventilation and perfusion pet/ct allows for functionally adapted intensity modulated radiotherapy in lung cancer,” Radiotherapy and Oncology, vol. 115, no. 2, pp. 157–162, 5 2015. [PubMed: 25935743]

[29]. Siva S, Devereux T, Ball DL, MacManus MP, Hardcastle N, Kron T et al., “Ga-68 maa perfusion 4d-pet/ct scanning allows for functional lung avoidance using conformal radiation therapy planning,” Technology in Cancer Research and Treatment, vol. 15, no. 1, pp. 114–121, 2 2016. [PubMed: 25575575]

[30]. Yaremko BP, Guerrero TM, Noyola-Martinez J, Guerra R, Lege DG, Nguyen LT et al., “Reduction of normal lung irradiation in locally advanced non-small-cell lung cancer patients, using ventilation images for functional avoidance,” International Journal of Radiation Oncology*Biology*Physics, vol. 68, no. 2, pp. 562–571, 2007.

[31]. Huang T-C, Hsiao C-Y, Chien C-R, Liang J-A, Shih T-C, and Zhang GG, “Imrt treatment plans and functional planning with functional lung imaging from 4d-ct for thoracic cancer patients,” Radiation oncology, vol. 8, no. 1, p. 3, 2013. [PubMed: 23281734]

[32]. Vinogradskiy Y, Schubert L, Diot Q, Waxweiller T, Koo P, Castillo R et al., “Regional lung function profiles of stage i and iii lung cancer patients: An evaluation for functional avoidance radiation therapy,” International Journal of Radiation Oncology, Biology, Physics, vol. 95, no. 4, pp. 1273–1280, 7 2016.

[33]. Yamamoto T, Kabus S, Bal M, Keall P, Benedict S, and Daly M, “The first patient treatment of computed tomography ventilation functional image-guided radiotherapy for lung cancer,” Radiotherapy and Oncology, vol. 118, no. 2, pp. 227–231, 2016. [PubMed: 26687903]

[34]. Yamamoto T, Kabus S, Bal M, Bzdusek K, Keall PJ, Wright C et al., “Changes in regional ventilation during treatment and dosimetric advantages of ct ventilation image-guided radiotherapy for locally advanced lung cancer,” International Journal of Radiation Oncology, Biology, Physics, 2018.

[35]. Castillo E, Castillo R, Vinogradskiy Y, and Guerrero T, “The numerical stability of transformation-based ct ventilation,” International Journal of Computer Assisted Radiology and Surgery, vol. 12, no. 4, pp. 569–580, 2017. [PubMed: 28058533]

[36]. Yamamoto T, Kabus S, Von Berg J, Lorenz C, Chung MP, Hong JC et al., “Reproducibility of four-dimensional computed tomography-based lung ventilation imaging,” Academic Radiology, vol. 19, no. 12, pp. 1554–1565, 2012. [PubMed: 22975070]

[37]. Shao W, Gerard SE, Pan Y, Patton TJ, Reinhardt JM, Durumeric OC et al., “Sensitivity analysis of jacobian determinant used in treatment planning for lung cancer,” in Proceedings of SPIE, vol. 10574 SPIE, 2018, pp. 1057 418–1057 418–9.

[38]. Klein S, Staring M, Murphy K, Viergever MA, and Pluim JP, “Elastix: A toolbox for intensity-based medical image registration,” IEEE Transactions on Medical Imaging, vol. 29, no. 1, pp. 196–205, 2010. [PubMed: 19923044]

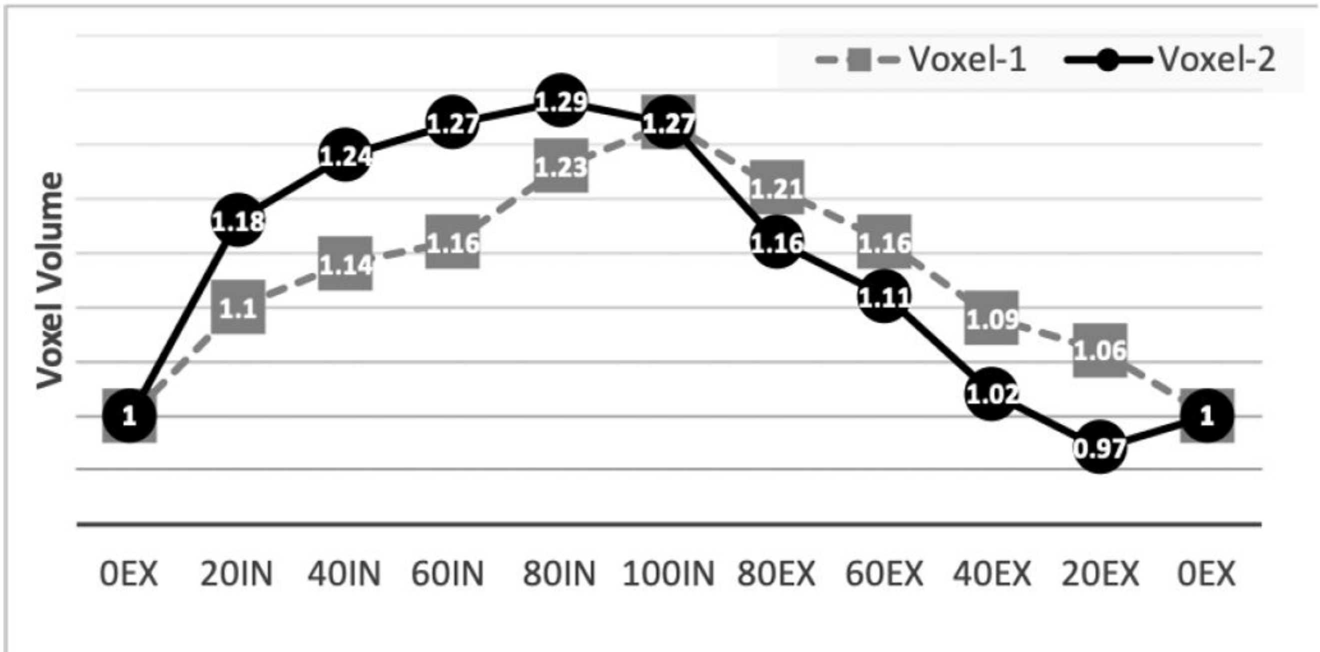

Fig. 1:

Typical in-phase and out-of-phase expansion and contraction that occurs during normal tidal breathing in a human subject. Voxel-1 has in-phase ventilation whereas Voxel-2 has out-of-phase ventilation. The 10 phases shown represent a breathing cycle. The suffix IN and EX correspond to inspiration and expiration phases, respectively. The prefix of each phase represents the percent inflation of the whole lungs normalized from end exhale (0%) to end inhale (100%). Notice that the y-axis of relative voxel volumes is unitless.

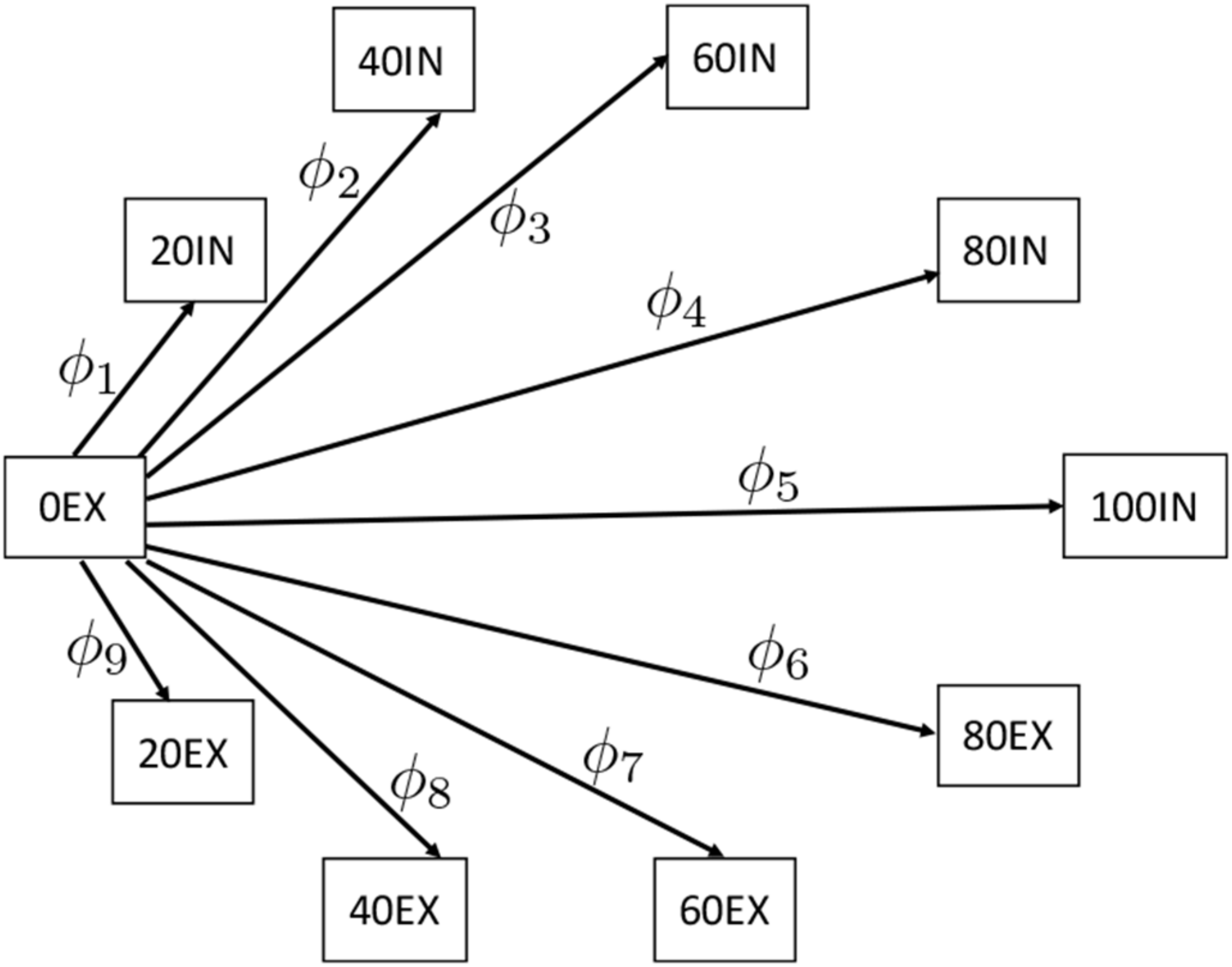

Fig. 2:
Pairwise registration from each breathing phase to the 0EX phase used to calculate LER_{10}.

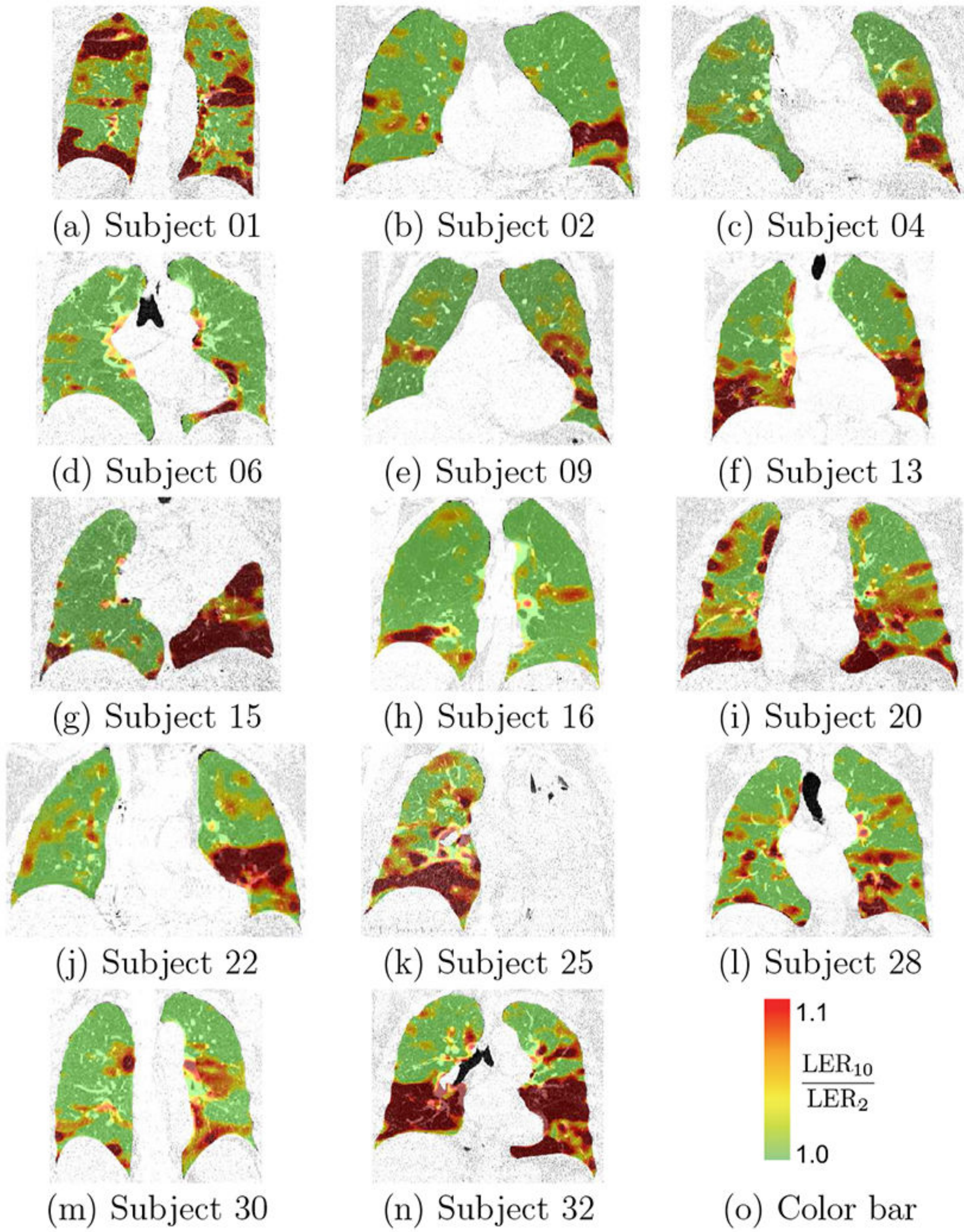

Fig. 3:

Out-of-phase ventilation images for 14 subjects. Regions of the lung that show in-phase (green), in-phase to out-of-phase transition (yellow to orange) and out-of-phase (red) breathing, respectively. These images show the ratio of LER_{10} to LER_2 overlaid on coronal CT images. The left lung of Subject 25 had been surgically removed.

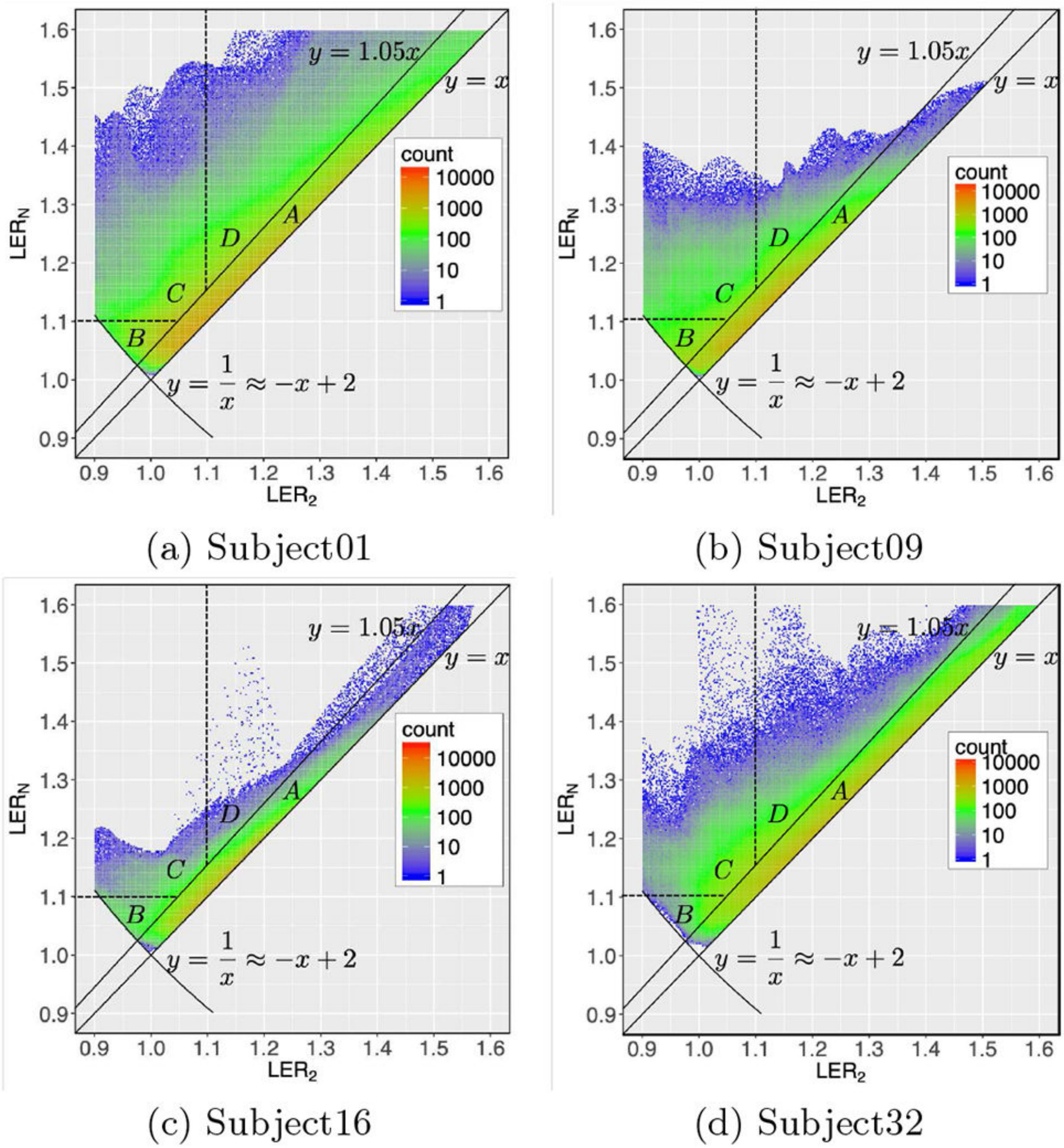

Fig. 4:

In-phase/out-of-phase ventilation (IOV) plots for four subjects. A logarithmic scale was used for visualization. LER_2 characterizes points to the right of the 1.1 vertical dashed line as high function and to the left as low function. LER_{10} characterizes points above the 1.1 horizontal dashed line high function and below as low function. Region A corresponds to lung regions with in-phase ventilation and regions B, C and D correspond to lung regions with out-of-phase ventilation.

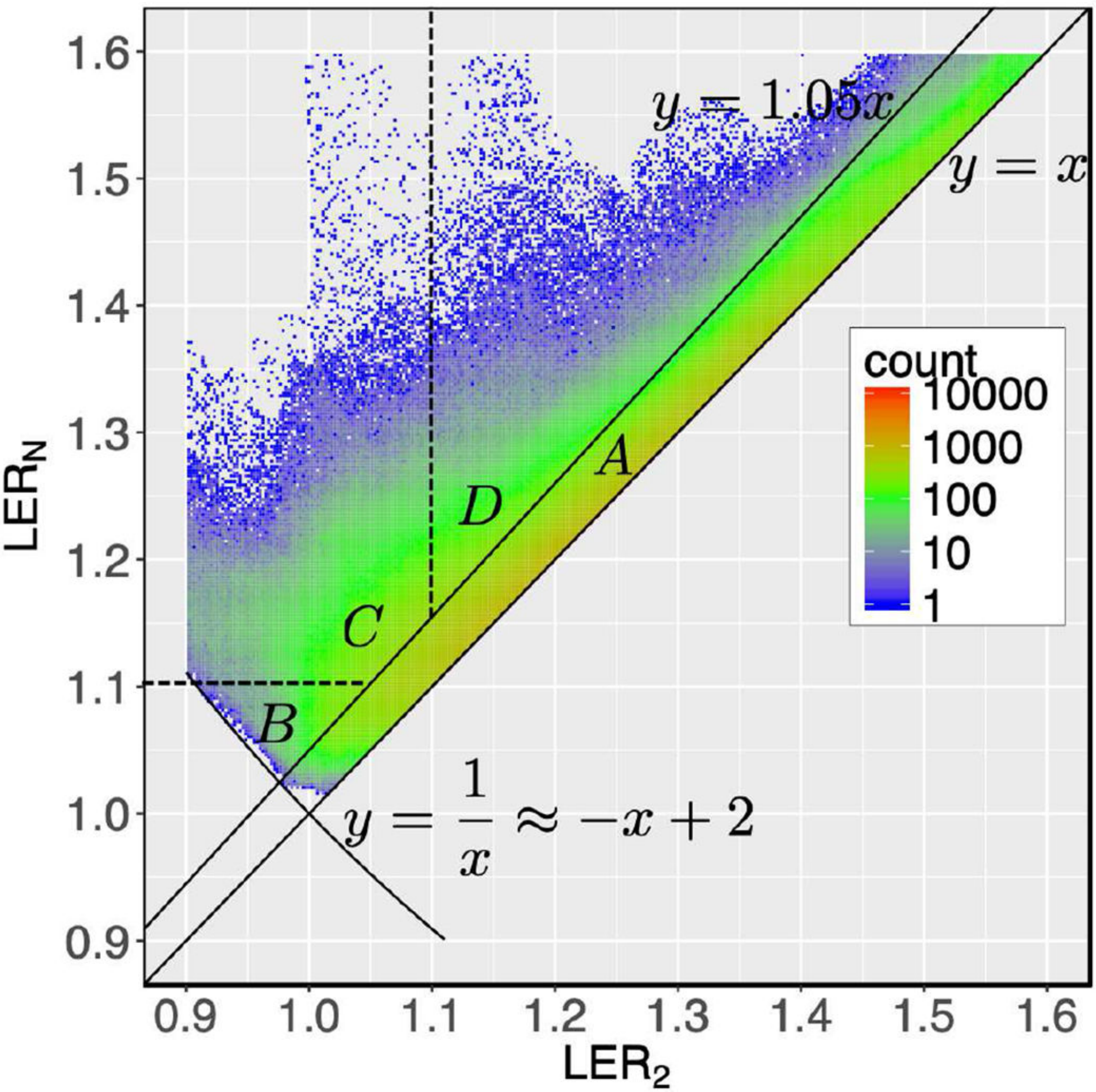

Fig. 5:
IOV function plot computed from all 32 subjects.

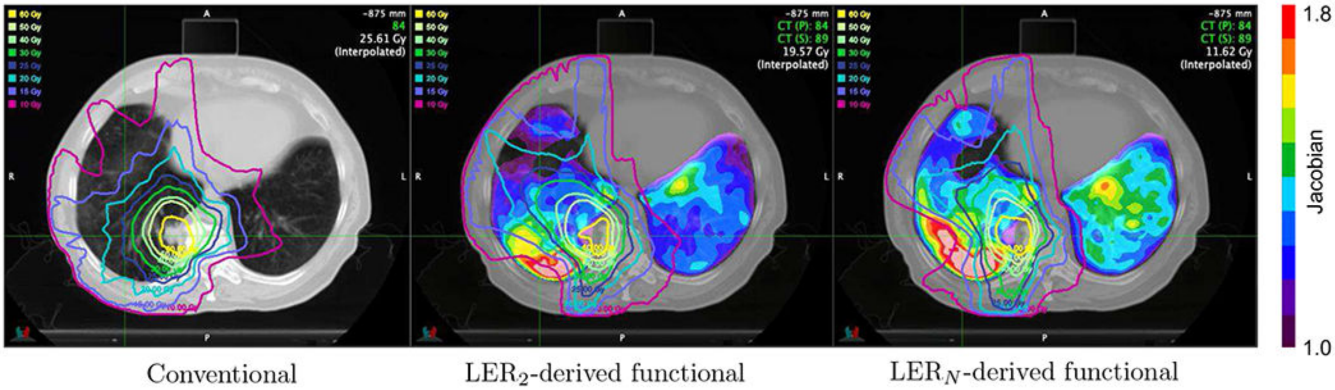

Fig. 6:

Transverse CT images of the lung of a patient with lung cancer. Overlaid contours show the isodose curves for conventional, LER$_2$-derived functional avoidance, and LER$_N$-derived functional avoidance dose plans. The smallest isodose curve (yellow) encompasses the tumor. The colored regions show the functional avoidance maps. Red corresponds to high function whereas purple and blue corresponds to low function.

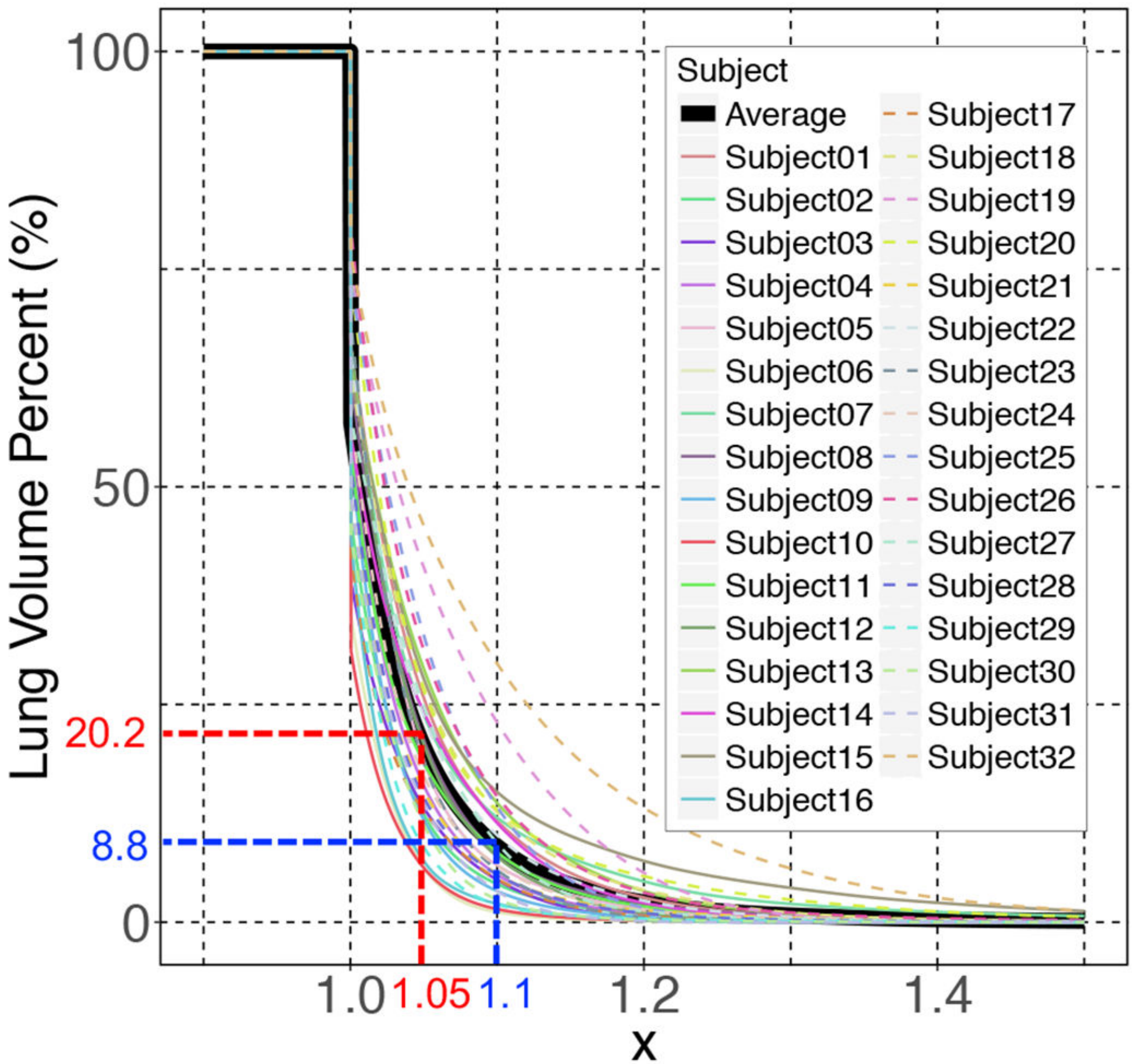

Fig. 7:
IOV threshold sensitivity plots for 32 subjects. A IOV threshold sensitivity plot shows the percentage of the lung that is considered out-of-phase for a particular IOV threshold T, i.e., regions where $LER_{10} > T \times LER_2$. The thick black line corresponds to the average of the 32 plots.

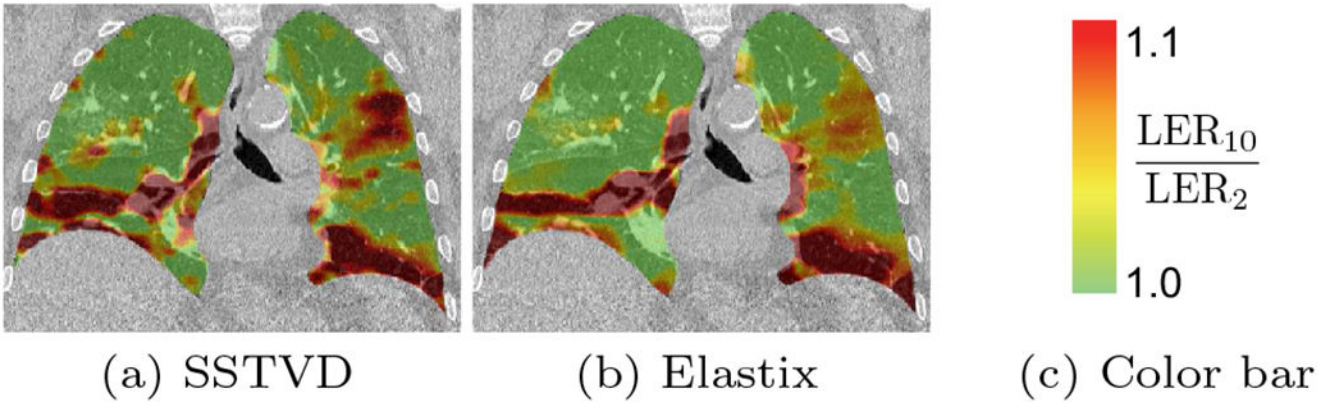

Fig. 8:

Comparison of the out-of-phase ventilation images of a typical subject computed by the SSTVD and Elastix algorithms.

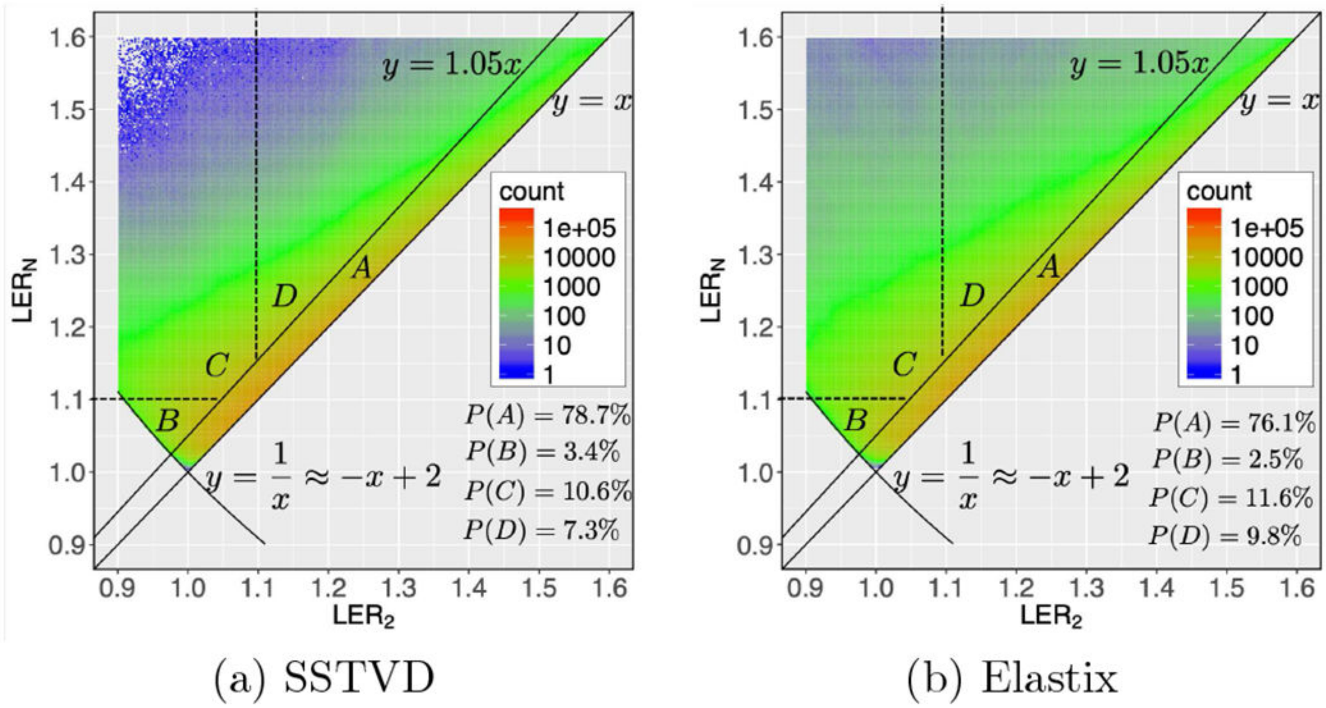

Fig. 9:

Comparison of the IOV function plot computed by the SSTVD and Elastix algorithms, respectively.

TABLE I:

Percentages of total lung volume for regions A, B, C and D for each subject. Region A is where the lung has in-phase ventilation, region B, C and D are regions where the lung has out-of-phase ventilation. The lung is characterized as low-function by both LER_2 and LER_{10} in region B, the the lung is characterized as as low-function by LER_2 whereas high-function by LER_{10} in region C, the lung is characterized as high-function by both LER_2 and LER_{10} in region D.

Region \ Subject	01	02	03	04	05	06	07	08	09	10	11
A	74.2	87.6	86.8	84.3	81.4	93.7	76.2	79.1	88.2	93.7	81.7
B	3.8	0.8	0.5	3.9	1.7	0.4	6.3	2.7	1.8	1.2	0.9
C	10.3	6.0	3.4	6.2	7.5	1.4	12.6	13	6.1	2.1	5.0
D	11.7	5.6	9.3	5.6	9.4	4.5	4.9	5.2	3.9	3.0	12.4
Region \ Subject	**12**	**13**	**14**	**15**	**16**	**17**	**18**	**19**	**20**	**21**	**22**
A	79.6	70.9	75.9	72.0	93.0	87.2	73.0	59.2	73.3	84.9	76.4
B	5.4	5.2	3.1	5.9	2.9	1.0	1.8	3.6	3.7	0.4	4.2
C	7.4	18.0	12.6	17.4	3.2	6.0	12.9	27.7	15.4	3.5	11.9
D	7.6	5.9	8.4	4.7	0.9	5.8	12.3	9.5	7.6	11.2	7.5
Region \ Subject	**23**	**24**	**25**	**26**	**27**	**28**	**29**	**30**	**31**	**32**	**Average**
A	81.6	83.1	67.0	68.7	75.2	85.7	91.4	88.8	86.5	54.4	79.8 ± 9.6
B	3.4	1.3	2.1	12.1	6.0	0.3	0.2	1.7	0.5	7.4	3.0 ± 2.6
C	10.1	8.8	17.5	17.7	7.5	2.2	1.2	4.2	2.8	31.5	9.8 ± 7.3
D	4.9	6.8	13.4	1.5	11.3	11.8	7.2	5.3	10.2	6.7	7.4 ± 3.3

TABLE II:

Spearman's correlation coefficients for the sheep experiment. The correlation coefficients in this table show that ventilation estimated using LER_8 is more correlated with Xe-CT specific ventilation than using LER_2. Statistical testing shows that LER_8 has a significantly (p-value = 0.04) higher correlation coefficient than LER_2.

Sheep	01	02	03	04	Mean
LER_2	0.418	0.635	0.336	0.356	0.436
LER_8	0.449	0.681	0.396	0.417	0.486